JB
Journals.ASM.org

A Cluster of Four Homologous Small RNAs Modulates C_1 Metabolism and the Pyruvate Dehydrogenase Complex in *Rhodobacter sphaeroides* under Various Stress Conditions

Fabian Billenkamp, Tao Peng, Bork A. Berghoff,* Gabriele Klug

Institut für Mikrobiologie und Molekularbiologie, Interdisziplinäres Forschungszentrum, Justus-Liebig-Universität Giessen, Giessen, Germany

ABSTRACT

In bacteria, regulatory RNAs play an important role in the regulation and balancing of many cellular processes and stress responses. Among these regulatory RNAs, *trans*-encoded small RNAs (sRNAs) are of particular interest since one sRNA can lead to the regulation of multiple target mRNAs. In the purple bacterium *Rhodobacter sphaeroides*, several sRNAs are induced by oxidative stress. In this study, we focused on the functional characterization of four homologous sRNAs that are cotranscribed with the gene for the conserved hypothetical protein RSP_6037, a genetic arrangement described for only a few sRNAs until now. Each of the four sRNAs is characterized by two stem-loops that carry CCUCCUCCC motifs in their loops. They are induced under oxidative stress, as well as by various other stress conditions, and were therefore renamed here sRNAs CcsR1 to CcsR4 (CcsR1–4) for conserved CCUCCUCCC motif stress-induced RNAs 1 to 4. Increased CcsR1–4 expression decreases the expression of genes involved in C_1 metabolism or encoding components of the pyruvate dehydrogenase complex either directly by binding to their target mRNAs or indirectly. One of the CcsR1–4 target mRNAs encodes the transcriptional regulator FlhR, an activator of glutathione-dependent methanol/formaldehyde metabolism. Downregulation of this glutathione-dependent pathway increases the pool of glutathione, which helps to counteract oxidative stress. The FlhR-dependent downregulation of the pyruvate dehydrogenase complex reduces a primary target of reactive oxygen species and reduces aerobic electron transport, a main source of reactive oxygen species. Our findings reveal a previously unknown strategy used by bacteria to counteract oxidative stress.

IMPORTANCE

Phototrophic organisms have to cope with photo-oxidative stress due to the function of chlorophylls as photosensitizers for the formation of singlet oxygen. Our study assigns an important role in photo-oxidative stress resistance to a cluster of four homologous sRNAs in the anoxygenic phototrophic bacterium *Rhodobacter sphaeroides*. We reveal a function of these regulatory RNAs in the fine-tuning of C_1 metabolism. A model that relates oxidative stress defense to C_1 metabolism is presented.

The purple bacterium *Rhodobacter sphaeroides* is able to adapt its life-style to changing environmental conditions by making use of many different metabolic pathways like aerobic and anaerobic respiration, fermentation, and anaerobic anoxygenic photosynthesis. Major determinants of the life-style of *R. sphaeroides* are light quality and quantity, as well as oxygen tension. Under microaerobic conditions, *R. sphaeroides* produces photosynthetic complexes in the dark, while light inhibits their formation (1, 2). In addition to the intricate transcriptional regulation of photosynthesis genes by diverse protein regulators, photosynthetic complex formation is also based on oxygen-dependent mRNA stability for photosynthetically relevant genes and control by sRNAs (3, 4). Light-dependent inhibition of photosynthetic complex formation in the presence of oxygen presumably avoids the formation of reactive oxygen species (ROS). The formation of most ROS (superoxide, hydrogen peroxide, and hydroxyl radicals) is based on electron transfer to molecular oxygen and can occur during aerobic respiration, as well as during photosynthesis (5). In contrast, singlet oxygen ($^1O_2$) is generated upon excitement transfer from a photosensitizer to molecular oxygen. In *R. sphaeroides*, it was shown that $^1O_2$ is generated in considerable amounts by bacteriochlorophylls of the reaction center (6, 7). $^1O_2$ can lead to the damage of various macromolecules within the cell and triggers a special set of sigma factors, which consequently leads to the activation of specific defense mechanisms (8). In addition to the major determinants, light and oxygen, further environmental factors like available carbon sources influence the life-style of *R. sphaeroides*. One carbon source that can be used under phototrophic, as well as respiratory, conditions is methanol (9–11). Throughout the utilization of this one-carbon (C_1) compound, the cytotoxic interme-

Received 6 November 2014 **Accepted** 9 March 2015

Accepted manuscript posted online 16 March 2015

Citation Billenkamp F, Peng T, Berghoff BA, Klug G. 2015. A cluster of four homologous small RNAs modulates C_1 metabolism and the pyruvate dehydrogenase complex in *Rhodobacter sphaeroides* under various stress conditions. J Bacteriol 197:1839–1852. doi:10.1128/JB.02475-14.

Editor: W. W. Metcalf

Address correspondence to Gabriele Klug, Gabriele.Klug@mikro.bio.uni-giessen.de.

* Present address: Bork A. Berghoff, Department of Cell and Molecular Biology, Biomedical Center, Uppsala University, Uppsala, Sweden.

F.B. and T.P. contributed equally to this work.

Supplemental material for this article may be found at http://dx.doi.org/10.1128/JB.02475-14.

doi:10.1128/JB.02475-14

diate formaldehyde is produced and is then degraded by a strictly regulated and glutathione (GSH)-dependent pathway (9, 12). In addition to the toxicity of formaldehyde, this metabolic pathway is another putative source of ROS. The transfer of reducing power to cytochromes and isocytochromes in the membrane by a pyrroloquinoline quinone (PQQ)-dependent pathway can result in the activation of an electron transport chain that uses molecular oxygen as a final electron acceptor (13). Consequently, the utilization of C_1 compounds might impact the redox status and indirectly cause ROS generation.

In many bacteria, small RNAs (sRNAs) play important roles in the regulation of stress responses, cell membrane modulation, carbon utilization, and other key events in the cell and finally support adaptation to changing environments (14). sRNA-dependent regulation relies on diverse mechanisms that occur mostly on the posttranscriptional level and include interaction with target mRNAs, as well as protein sequestering. Interaction with target mRNAs can affect mRNA stability and/or translation initiation (14). Often, the bacterial Sm-like protein Hfq is needed to enable base pairing between sRNAs and their target mRNAs. Hfq increases sRNA stability, solves secondary structures in sRNAs, as well as in mRNAs, and finally helps sRNAs to bind their target mRNAs (15–18). By a differential RNA sequencing (dRNA-seq) (19) approach searching for photo-oxidative stress-related and abundant sRNAs in *R. sphaeroides*, 20 sRNAs were identified (20). Many of these sRNAs are induced upon stress, and their transcription is initiated at distinct promoters that are recognized by alternative sigma factors. For example, the alternative sigma factor RpoE is activated by $^1O_2$ and subsequently induces one sRNA, as well as another sigma factor, $RpoH_{II}$, which in turn induces three additional sRNAs (21). These findings imply that sRNAs support the regulation of stress responses in *R. sphaeroides*.

Among the sRNAs that are induced by different ROS, *R. sphaeroides* possesses a repeat of the four homologous sRNAs RSs0680a to RSs0680d (here renamed CcsR1 to CcsR4 [CcsR1–4] for conserved CCUCCUCCC motif stress-induced RNAs 1 to 4), which are cotranscribed with an upstream gene, encoding a hypothetical protein (RSP_6037) (20). This protein contains a conserved domain of unknown function (DUF1127). In *R. sphaeroides*, the RSP_6037–CcsR1–4 operon is controlled by a promoter that is dependent on both $RpoH_I$ and $RpoH_{II}$, which leads to induction under multiple stress conditions like oxidative and photo-oxidative stress but also under heat stress (20, 21). In this study, we focused on the function of sRNAs CcsR1–4 and found that they modulate methanol-based C_1 metabolism under oxidative stress conditions. This presumably leads to an increase in the availability of major scavengers of ROS like reduced GSH and also reduces sources of oxidative stress derived from C_1 metabolism. Moreover, we found indications that CcsR1–4 are involved in stress-dependent downregulation of the pyruvate dehydrogenase complex. Our data indicate that functional cooperation among the four homologous sRNAs exists and that they might collaboratively act under stress conditions.

MATERIALS AND METHODS

Construction of CcsR-overexpression strains. In order to construct bacterial strains with enhanced levels of CcsR RNAs, we made use of overexpression plasmids pRK4352 and pBBR4352 (4). A DNA fragment containing the promoterless RSP_6037–CcsR1–4 locus was PCR amplified, subcloned into the pDrive cloning vector (Qiagen), and ligated into the BamHI/EcoRI sites of pRK4352 after restriction with the corresponding enzymes. The resulting plasmid was named pR6037_CcsR1–4. Smaller DNA fragments, comprising solely CcsR1–4, were cloned in a similar way into the BamHI/EcoRI and BamHI/XbaI sites of pRK4352 and pBBR4352, yielding plasmids pRCcsR1–4 and pBCcsR1–4, respectively. For overexpression of CcsR1, CcsR2, CcsR1 and CcsR2, and CcsR1 to CcsR3, cloning into pRK4352 was done as described and the plasmids obtained were named pRCcsR1, pRCcsR2, pRCcsR1+2, and pRCcsR1–3. All plasmids were transferred to *R. sphaeroides* by conjugation. For the primers and plasmids used, see Tables S1 and S2 in the supplemental material.

Deletion of *flhR*. The protein-coding sequence of *flhR* was completely deleted and replaced with the kanamycin resistance cassette from pUC4K (22). A 688-bp DNA fragment located upstream of *flhR* was amplified with primers up2591Kpn-f and up2591Pst-r (see Table S1 in the supplemental material). A 682-nucleotide (nt) DNA fragment located downstream of *flhR* was amplified with primers down2591Pst-f and down2591Hind-r. The *flhR* downstream fragment was cloned into the HindIII and PstI sites of plasmid pPHU281 (23); afterwards, the upstream fragment was introduced into the KpnI and PstI sites. The kanamycin cassette from pUC4K was cloned into the PstI site. The resulting plasmid, pPHU2591up-KM-down, was transferred into *R. sphaeroides* 2.4.1 by conjugation, and kanamycin-resistant and tetracycline-sensitive clones were selected. Correct insertion of the kanamycin resistance cassette into the chromosome by double crossover was confirmed by PCR with suitable primers.

Construction of an FlhR expression plasmid. The protein-coding sequence of *flhR*, together with the 5′ untranslated region (UTR), was amplified with primers 2591ovfbam1 and 2591ovRkpn1 and introduced into the BamHI and KpnI sites of pRK4352 (4). The resulting plasmid, pRK_*flhR*, was transferred to wild-type *R. sphaeroides* 2.4.1 and an endogenous *flhR* deletion strain, and tetracycline-resistant clones were selected.

Construction of *lacZ* reporter plasmids. To analyze sRNA-mRNA interactions, the 16S rRNA (RSP_4352) promoter sequence was amplified and subcloned into the pDrive cloning vector (Qiagen). After restriction of the pDrive derivative with XhoI and KpnI, the promoter fragment was introduced into the corresponding restriction sites of the *lacZ* fusion vector pPHU235 (24), yielding plasmid pPHU16S. DNA fragments containing an upstream region and the first codons of genes with predicted mRNA interaction sites for CcsR1–4 were amplified with specific primers and subcloned into the pDrive cloning vector (Qiagen) or cloning vector pJET1.2 (Thermo Scientific). After restriction with XbaI and PstI, DNA fragments were cloned into plasmid pPHU16S, producing in-frame fusions to the *lacZ* gene. Reporter plasmids were finally transferred to *R. sphaeroides* strains harboring either pBBR4352 or pBCcsR1–4 by conjugation. For the primers and plasmids used, see Tables S1 and S2 in the supplemental material.

Site-directed mutagenesis. The derivative of pDrive containing the *flhR* (RSP_2591) fragment was used as the template for mutagenesis PCR. Primers Mut2591GGA27CCTfw and Mut2591GGA27CCTrv were designed to introduce specific mutations into the sRNA-mRNA interaction region of the mRNA. After PCR, template plasmids were digested with DpnI and PCR-generated (mutated) plasmids were transformed into *Escherichia coli* JM109. Successful mutagenesis was verified by sequencing. Finally, the mutated RSP_2591 (*flhR*) mRNA fragment was cloned into the XbaI/PstI sites of pPHU16S, resulting in $pPHU16S2591_{mut3}$.

Bacterial strains and cultivation. Precultures of *R. sphaeroides* were grown in minimal-salt medium containing malate as a carbon source at 32°C under microaerobic conditions (25 μM dissolved oxygen) by shaking flasks filled to 75% of their respective volume at 140 rpm (25). Experiments were performed under either microaerobic or aerobic conditions (180 μM dissolved oxygen; continuous aeration). The strains used in this work were wild-type *R. sphaeroides* 2.4.1 and derivatives thereof (see Table S3 in the supplemental material). For cloning procedures, *E. coli* strains JM109 and S17-1 (see Table S3) were grown in Standard I nutrient broth (Roth) at 37°C under aerobic conditions. Antibiotics were applied to *R.*

sphaeroides and *E. coli* cultures when necessary. For the final concentrations used, see Table S3.

Physiological experiments. *R. sphaeroides* cultures were grown under either aerobic or microaerobic conditions and harvested at an optical density at 600 nm (OD_{660}) of 0.4 (exponential growth phase) or 1.5 (transition to stationary growth phase under microaerobic and aerobic growth conditions) for analysis of growth phase-dependent CcsR1–4 expression. For analysis of the (photo-)oxidative stress response, cultures were grown in minimal-salt medium under aerobic conditions as described above. At an OD_{660} of 0.4 (exponential growth phase), 250 μM paraquat, 100 μM *tert*-butyl hydroperoxide (tBOOH), or 1 mM hydrogen peroxide (H_2O_2) was added (time point 0) and cells were incubated with the stress-generating chemical for 10 min. Photo-oxidative stress was generated by the addition of 0.2 μM methylene blue and irradiation with white light at 800 W/m^2 for 10 min as described previously (26). Cultures for salt and heavy metal experiments were grown under microaerobic conditions to an OD_{660} of 0.4 as described above and supplemented with 10 μM cadmium chloride, 100 μM zinc sulfate, or 500 mM sodium chloride for 10 min until harvesting. For analysis of the heat shock response, cells were grown at 32°C under microaerobic conditions and shifted to a water bath at 42°C for 10 min when an OD_{660} of 0.4 was reached. Cells were harvested on ice and collected by centrifugation at 10,000 × *g* and 4°C.

Zone-of-inhibition assays. For zone-of-inhibition assays, overnight cultures of *R. sphaeroides* were diluted to an OD_{660} of 0.2 and cultivated under microaerobic conditions as described above. After they reached an OD_{660} of 0.4, cultures were harvested and diluted to an OD_{660} of 0.2. Seven milliliters of top agar (minimal-salt medium containing 0.8% agarose) was mixed with 200 μl of diluted culture and poured on top of an agar plate (1.6% agarose in minimal-salt medium) without a selection marker. After solidification of the top agar, filter disks soaked with either 10 μl of 700 mM tBOOH or 10 μl of 200 mM paraquat were placed on top of the plates. After incubation at 32°C for 3 days, the diameters of the inhibition zones were measured.

RNA preparation. For Northern blot analysis, total RNA was isolated by the hot-phenol method (27) and quantified photometrically at 260 nm with a NanoDrop 1000 UV/Vis spectrophotometer (PeqLab). For transcriptome analysis, total RNA was isolated as described previously (28). In short, RNA was extracted by the hot-phenol method and contaminating DNA was removed by DNase I (Invitrogen) treatment. Afterwards, RNA was purified with RNeasy MinElute spin columns (Qiagen) and RNA quality was assigned on 10% polyacrylamide gels.

Northern blot analysis. Total RNA was separated on 10% polyacrylamide gels containing 7 M urea. RNA was transferred to nylon membranes by semidry electroblotting as described previously (20). For detection of CcsR1 in initial experiments, the 24-nt antisense oligodeoxynucleotide p-0680a (see Table S1 in the supplemental material), which binds to the second stem-loop of the sRNA, was used. For differential detection of CcsR1 to CcsR3, antisense oligodeoxynucleotides for the respective full-length sRNAs were used (see Table S1). RSs1543 and 5S rRNA were detected with probes p-1543 and p-5S. Oligodeoxynucleotides were end labeled with [γ-^{32}P]ATP and T4 polynucleotide kinase (Fermentas) and subsequently purified with Microspin G-25 columns (GE Healthcare). Hybridization was performed in accordance with the protocol of Church and Gilbert for hybridization buffer with low and moderate stringency (29).

Transcriptome analysis. For microarray analysis, strains were grown under aerobic conditions to exponential phase (OD_{660} of 0.4). Two individual microarrays (biological replicates), each containing a pool of three independent experiments for each strain, were applied as follows. Two micrograms of pooled total RNA from *R. sphaeroides* strains 2.4.1(pRK415) and 2.4.1(pRCcsR1–4) was labeled with Cy5 and Cy3, respectively, with the ULS Fluorescent Labeling kit for Agilent arrays (Kreatech) and competitively hybridized to Custom Gene Expression Microarrays from Agilent Technologies (8x15K; ID 027061) designed for wild-type *R. sphaeroides* 2.4.1 (28). Sample fragmentation, hybridization, and data scanning were performed in accordance with the specifications given by Agilent. Raw median fluorescence values were extracted with the Feature Extraction Software (Agilent), and data were further processed with the Bioconductor package Limma for R (30). Within-array normalization according to LOESS corrected for dye bias. Normalized fluorescence values were used to calculate expression ratios. Only probes with fluorescence values above the background, as specified by nonspecific probes, were included in the analysis. In order to filter for genes with differential expression, only probes giving a $\log_2$ ratio of ≤ -0.7 or ≥ 0.7 were included, while the remaining probes were omitted. Finally, genes of special interest after bioinformatic analyses for RNA interaction of CcsR1–4 with respective with mRNAs (see below) were analyzed manually.

qRT-PCR. RNA was prepared by the hot-phenol method as described above. The One-Step Brilliant III quantitative reverse transcription (qRT)-PCR master mix kit (Agilent) was used for RT, followed by PCR as described in the manufacturer's manual. A final concentration of 4 ng of total RNA μl^{-1} was used. Reactions were run in a C1000 thermal cycler (Bio-Rad Laboratories). For the primers used for amplification, see Table S1 in the supplemental material. Expression of mRNAs was calculated relative to that of a control sample and normalized to *rpoZ*. Statistical analysis was performed with Student's *t* test, and *P* values of ≤ 0.05 were considered statistically significant.

Proteome analysis. Cultures of *R. sphaeroides* 2.4.1(pRK415) and 2.4.1(pRCcsR1–4) were grown under aerobic conditions to the exponential growth phase (OD_{660} of 0.4). Soluble proteins from biological triplicates were subjected to gel-based proteomics after L-[^{35}S]methionine pulse-labeling as described previously (31). Evaluation of protein gels was performed with Delta2D software (Decodon) (32).

Gel mobility shift assay. RNAs were transcribed *in vitro* with T7 RNA polymerase (New England BioLabs) by using PCR products with T7 promoter sequences in the 5′ end as templates. For the primers used to generate DNA templates for *in vitro* transcription of CcsR1, PcrZ (control sRNA), *flhR* (target mRNA), and *bchN* (control mRNA), see Table S1 in the supplemental material. CcsR1 and PcrZ were labeled with [α-^{32}P]UTP in the reaction mixture, while mRNA fragments remained unlabeled. After transcription, the RNA was purified with G50 spin columns (GE Healthcare) followed by gel extraction. RNA interactions were tested in a final volume of 15 μl by mixing 250 fmol of sRNA (CcsR1 or PcrZ) with various amounts of mRNA. Samples were incubated in 1× structure buffer (100 mM Tris [pH 7], 1 M KCl, 100 mM $MgCl_2$) for 30 min at 32°C. Reaction mixtures were then mixed with 3 μl of loading dye (50% glycerol, 0.5× Tris-borate-EDTA [TBE], 0.2% bromophenol blue) and loaded onto native gels containing 0.5× TBE and 6% acrylamide. Gels were prerun at 100 V for 30 min before loading. Electrophoresis was performed at room temperature by applying 200 V for 2.5 h. Gels were dried and analyzed via phosphorimaging.

Bioinformatic tools. The prediction of sRNA structures was performed with Sfold and RNAfold (33–35). For putative CcsR1–4 targets, mRNA structures were predicted with the NUPACK webserver similarly to previous studies (36, 37). The analysis was done by using standard parameters for NUPACK but changing the environmental temperature to 32°C, reflecting the regular incubation temperature of *R. sphaeroides* under laboratory conditions. Genome-wide predictions of sRNA-mRNA interactions were performed with IntaRNA and RNApredator (38, 39). The top 50 results of each search were subjected to further analysis. For analysis of operons, the Prokaryotic Operon DataBase (ProOpDB) was used (40).

Determination of β-galactosidase activity in reporter strains. Derivatives of pPHU16S containing putative target mRNAs were introduced into *R. sphaeroides* strains carrying either pBBR4352 or pBCcsR1–4 by conjugation. Conjugants were cultivated on plates containing appropriate mixtures of antibiotics at 32°C. Three liquid cultures were derived for each reporter strain by inoculating a mixture of 10 colonies/conjugants. These cultures were used to measure the relative β-galactosidase activity in the

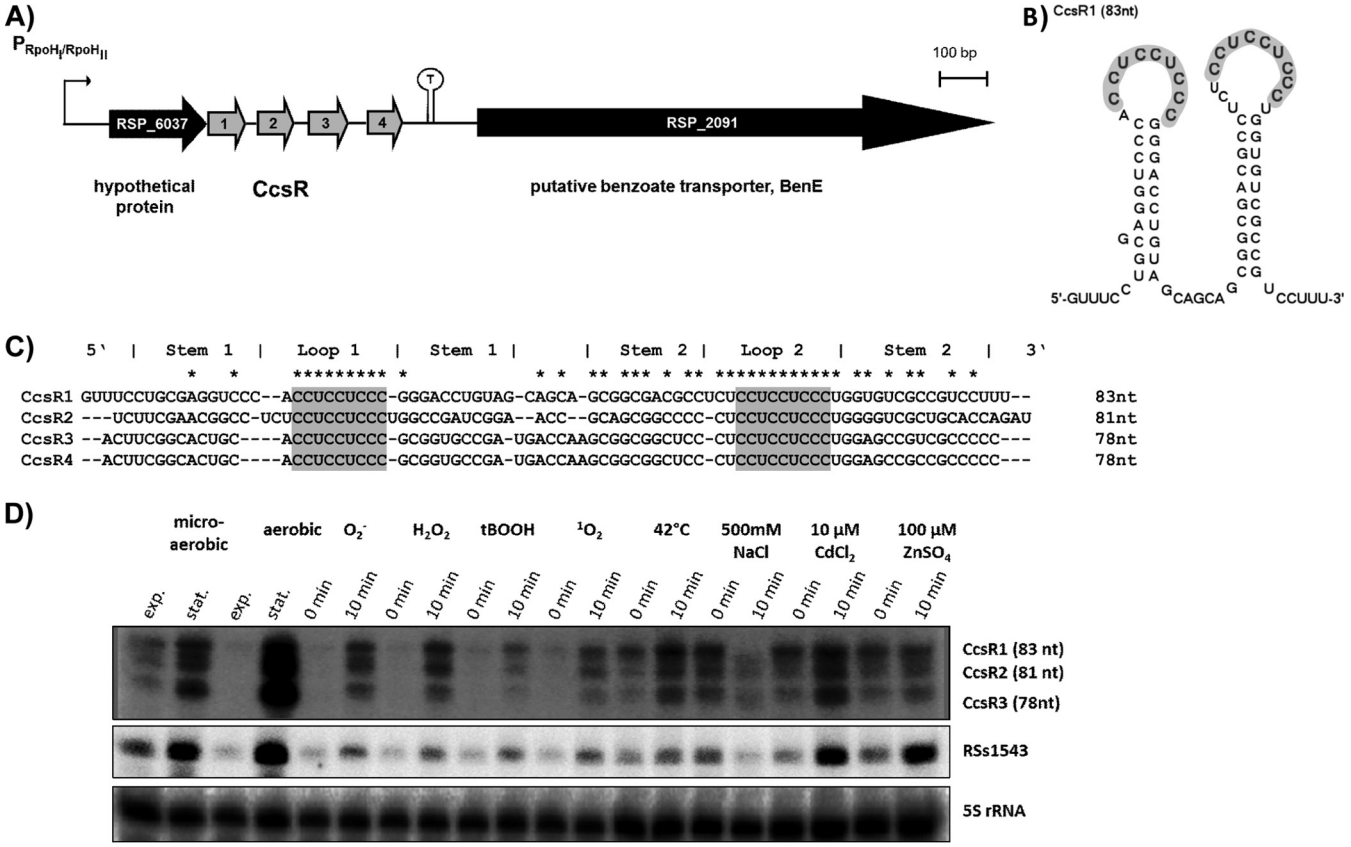

FIG 1 Expression conditions for the homologous CcsR sRNAs. (A) The four sRNAs CcsR1–4 are transcribed together with an upstream gene encoding a conserved hypothetical protein (RSP_6037). Transcription is initiated at an $RpoH_I/RpoH_{II}$-dependent promoter and terminated at a rho-independent stem-loop structure (20). (B) The secondary structure of CcsR1 displays two exposed CCUCCUCCC motifs in the loops (gray). The secondary structure was predicted by Sfold (33). (C) Alignment of CcsR1–4 sequences. Albeit showing a similar secondary structure, only the CCUCCUCCC motifs (gray) are highly conserved. Perfect conservation among all four sRNAs is indicated by asterisks. (D) Differential detection of CcsR1, CcsR2, and CcsR3 and CcsR4 in Northern blot assays. CcsR1–4 levels were monitored under different growth/stress conditions: exponential (exp.) and stationary (stat.) growth phases under aerobic and microaerobic conditions; O_2^-, superoxide (250 µM paraquat, aerobic conditions); 1 mM H_2O_2, aerobic conditions; 100 µM tBOOH, aerobic conditions; $^1O_2$, singlet oxygen (0.2 µM methylene blue, white light at 800 W/m^2, aerobic conditions); 42°C, heat stress (microaerobic conditions); 500 mM NaCl, salt stress (microaerobic conditions); 10 µM $CdCl_2$, cadmium stress (microaerobic conditions); 100 µM $ZnSO_4$, zinc stress (microaerobic conditions). Time point 0 min represents sRNA expression before the addition of chemicals to the liquid cultures, while time point 10 min is after 10 min of incubation with the chemical or at 42°C. RSs1543 and 5S rRNA were probed as controls. For detection of CcsR1 to CcsR3, the probes pCcsR1 (73 nt), pCcsR2 (80 nt), and pCcsR3 (88 nt) were used.

early exponential growth phase (OD_{660} of 0.4). Measurements of β-galactosidase activity were carried out as previously described (41, 42).

Determination of total GSH. For GSH assays, cultures were grown under microaerobic conditions to an OD_{660} of 0.4. Cells from 2 ml of culture were harvested on ice, and pellets were stored at −20°C after centrifugation at 10,000 × *g*. Cells were resuspended in 3.75% 5-sulfosalicylic acid for lysis, which was supported by vigorous shaking. Cell debris and proteins were precipitated by centrifugation at 10,000 × *g* and consequently separated from GSH, which remained in the supernatant. Ellman's reagent [5,5′-dithiobis-(2-nitrobenzoic acid) (DTNB)] was prepared as a 6 mM solution in reaction buffer (143 mM NaH_2PO_4, 6 mM EDTA, pH 7.5) and used for colorimetric determination of GSH. Reaction mixtures with a volume of 1 ml were set up as follows. An 845-µl volume of reaction buffer containing NADPH (0.3 mg ml^{-1}) was mixed with 50 µl of supernatant and 100 µl of DTNB (6 mM). Samples were kept at room temperature for 10 min to allow GSH to be completely oxidized by DTNB. Afterwards, reactions were started by adding 5 µl of GSH reductase from baker's yeast (Sigma-Aldrich; diluted to 100 U ml^{-1} in reaction buffer). Color development was monitored at 412 nm over time. Total GSH concentrations were calculated from initial slopes in comparison to a calibration curve prepared from a standard GSH solution in reaction buffer. Total GSH concentrations were normalized to OD_{660} values.

Microarray data accession number. The data discussed in this publication have been deposited in the NCBI Gene Expression Omnibus and are accessible through GEO Series accession number GSE67145 (43).

RESULTS

The CcsR sRNAs contain conserved sequence motifs and are expressed under various stress conditions. The sRNAs CcsR1–4 were originally discovered by dRNA-seq and were shown to form an operon with the hypothetical protein RSP_6037 (Fig. 1A) (20). In a strain lacking the alternative sigma factors $RpoH_I$ and $RpoH_{II}$, decreased amounts of CcsR1 were detectable, in agreement with transcription from an $RpoH_I/RpoH_{II}$ promoter upstream of RSP_6037 and generation of CcsR1–4 by processing (21). On the basis of new sequencing results obtained with Illumina (data not shown) combined with the specific detection of individual sRNAs in Northern blot assays (see Fig. S1 in the supplemental material), we redefined their particular lengths: CcsR1 has a size of

83 nt (RSs0680a, 73 nt previously [20]), while CcsR2 has a size of 81 nt (RSs0680b, 80 nt previously [20]) and CcsR3 has a size of 78 nt (RSs0680c, 88 nt previously [20]). The size of CcsR4 could not be determined because of weak coverage in RNA-seq, but the data indicate a size of 78 nt, which is supported by a single band in Northern blot assays when using a probe against CcsR3 that also binds CcsR4 because of sequence identity (Fig. 1C; see Fig. S1). The predicted secondary structures of the sRNAs show high conservation. They consist of two stem-loop structures presenting non-base-paired CCUCCUCCC motifs on top of both stem-loops (Fig. 1B shows the folding of CcsR1; for the structures of CcsR2 and CcsR3, see Fig. S2A and S2B). The CCUCCUCCC motifs show high sequence conservation among CcsR1–4, while other bases of the sRNAs show only moderate conservation. Especially the bases involved in the formation of the first stem show only limited conservation, while the stem structure is nevertheless conserved (Fig. 1C). It was possible to detect CcsR1 and CcsR2 differentially in Northern blot assays with specific 70-nt probes (Fig. 1D; see Fig. S1), while individual detection of CcsR3 and CcsR4 failed because of particularly high sequence homology between the two sRNAs, as mentioned above (Fig. 1C). It was previously shown that singlet oxygen or heat shock leads to induction of CcsR1 expression (20, 21). In order to expand the knowledge about conditions that induce the expression of CcsR1–4, liquid cultures of wild-type *R. sphaeroides* 2.4.1 in the early exponential growth phase were subjected to different stress conditions. These experiments revealed that CcsR1–4 are strongly induced upon transfer to stationary phase and under various stress conditions. Especially (photo-)oxidative stress and heat shock led to induction of CcsR1–4, while salt stress led to a lower CcsR1–4 level. Moreover, a weak effect of cadmium ions on CcsR1–4 expression was observable (Fig. 1D). The sRNA RSs1543 (21), which is also under the control of an $RpoH_I$/$RpoH_{II}$-dependent promoter, showed the same induction pattern as observed for CcsR1–4. Since the basal expression levels of CcsR1–4 and RSs1543 depend on oxygen tension, the bands at time point 0 show different intensities and were higher at time point 0 under microaerobic conditions.

Overexpression of CcsR sRNAs leads to enhanced resistance to oxidative stress. To assess the function of the CcsR sRNAs, we first attempted to construct a strain that has CcsR1–4 deleted from the chromosome. It was not possible to isolate such a mutant, implying that CcsR1–4 are essential. If CcsR1–4 were provided on a plasmid, a deletion of the chromosomal copy was possible. We designed overexpression plasmids to alter the cellular CcsR1–4 levels. The CcsR1–4 sRNA cluster, either with or without the upstream RSP_6037 gene, was expressed under the control of a strong 16S rRNA promoter on the low-copy-number plasmid pRK415. The resulting plasmids (Fig. 2A) were transferred to wild-type *R. sphaeroides* 2.4.1 and an *hfq* deletion strain. Northern blot analysis with a probe that preferentially binds CcsR1 (p-0680a) demonstrated that the abundance of CcsR1 was influenced by the presence of RSP_6037: the sRNA abundance was decreased when RSP_6037 was simultaneously overexpressed (Fig. 2B). Furthermore, a positive influence of Hfq on steady-state CcsR1–4 levels was observed. Interaction of Hfq with CcsR1–4 was previously demonstrated (20, 44). Overexpression of CcsR1–4 had no significant impact on the growth rate under either aerobic or microaerobic conditions (data not shown). Interestingly, the resistance to oxidative stress was enhanced when overexpressing CcsR1–4 (Fig. 2C). The degree of enhancement of resistance was proportional to that of CcsR1–4 RNA levels and therefore was influenced by the simultaneous overexpression of RSP_6037 (compare Fig. 2B and C). We also tested strains overexpressing CcsR1 or CcsR2 alone, CcsR1 and CcsR2, or CcsR1 to CcsR3. All of the strains showed higher resistance to 200 mM paraquat than a control strain did. Maximal resistance was achieved only when all copies of CcsR were present (Fig. 2D). This indicates that CcsR contributes to stress resistance when only a single copy is present but that the presence of several copies enhances the function of CcsR.

CcsR1–4 target search by a combined approach. In order to better understand the function of CcsR1–4, we used a combined target search approach. The data from a microarray analysis, a proteome analysis of soluble proteins, and bioinformatic predictions were integrated, and putative targets of CcsR1–4 were selected for further analysis. In the microarray analysis, we compared wild-type *R. sphaeroides* strain 2.4.1, which constitutively overexpresses CcsR1–4 without RSP_6037, to an empty-vector control. Because of the constant overexpression of CcsR1–4, cells may adapt to this situation, so that the detection of direct but also indirect effects of CcsR1–4 can be expected. Only 1% of the transcripts analyzed with reliable A-value showed a considerable difference in expression levels. Only 0.4% of the transcripts showed higher abundance in the CcsR1–4 overexpression strain ($\log_2$ ratio of ≥ 0.7), and 0.5% of the transcripts showed a decreased level ($\log_2$ ratio of ≤ -0.7, see Fig. S3B). Among the transcripts with increased abundance, CcsR1 to CcsR3 showed the strongest upregulation (Fig. S3C), which was expected in the overexpression strain and underscores our Northern blot assay results (Fig. 2B). While no functional groups could be determined for genes with increased transcript levels, two functional groups emerged among the genes with lowered transcript levels. On the one hand, genes related to C_1 metabolism showed lower mRNA abundance, i.e., *pqqA* (RSP_6132, putative coenzyme PQQ synthesis protein), *xoxJ* (RSP_2580, putative methanol oxidation protein), *xoxF* (RSP_2578, putative PQQ dehydrogenase protein), *cycB* (RSP_2579, cytochrome c533i), and *coxS* and *coxL* (RSP_2878 and RSP_2877, two subunits of a putative carbon monoxide dehydrogenase). On the other hand, genes that encode subunits of the pyruvate dehydrogenase complex exhibited lower mRNA levels, i.e., *pdhD* (RSP_2968, dihydrolipoamide dehydrogenase), *pdhAb* (RSP_4049, dehydrolipoamide acetyltransferase), and *pdhB* (RSP_4050, deydrolipoamide acetyltransferase E2 component). Finally, four protein-coding genes and two sRNAs that do not belong to the groups mentioned were downregulated (Fig. S3C). The proteins encoded by these mRNAs resemble hypothetical proteins, a flagellum structure protein and a nucleotide sugar epimerase, while the function of the sRNAs is unknown. After evaluation of the microarray, we added data from a proteomic approach comparing the CcsR1–4 overexpression strain and the control strain, which we have already used for microarray analysis. Proteins were pulse-labeled with L-[^{35}S]methionine for 10 min, and changes in protein spots therefore reflect changes in protein synthesis (Fig. S3D). By this approach, we detected 511 protein spots. A significant decrease in spot intensity ($\log_2$ ratio of $\leq -0,3$; $P \leq 0.05$) in the CcsR1–4 overexpression strain could be detected for 18 protein spots, while a significant increase in spot intensity ($\log_2$ ratio of $\geq 0,3$; $P \leq 0.05$) could be detected for 5 protein spots. However, we found only a small direct overlap with the microarray data, which was limited to CoxL (RSP_2877). The synthesis of several proteins with roles in C_1 metabolism and the pyruvate

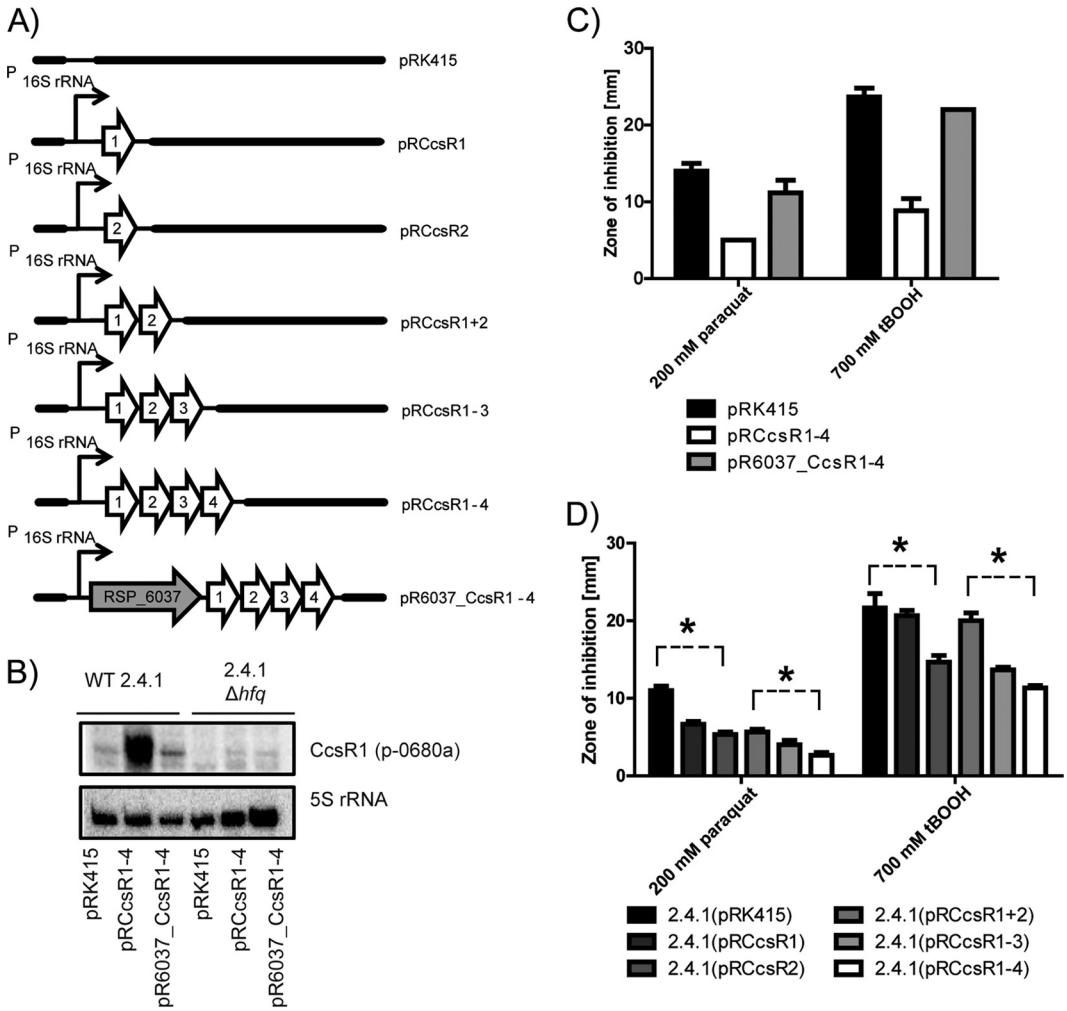

FIG 2 Expression of CcsR1–4 is RSP_6037 and Hfq dependent, and elevated levels of the four sRNAs lead to enhanced resistance to oxidative stress. (A) Schematic representation of plasmids used for constitutive overexpression of the CcsR RNAs under the control of the 16S rRNA promoter. The broad-host-range plasmid pRK415 was used as an empty-vector control. (B) The level of CcsR1 expression is decreased in an *hfq* deletion strain and is negatively influenced by co-overexpression with RSP_6037, as monitored by Northern blotting of total RNA from cultures in the exponential growth phase. Results for wild-type (WT) *R. sphaeroides* and an *hfq* deletion strain, each harboring plasmid pRK415, pRCcsR1–4, or pR6037_CcsR1–4, are shown. 5S rRNA served as a loading control. For detection of CcsR1, p-0680a was used. (C and D) Enhanced resistance to oxidative stress caused by paraquat or the organic hydroperoxide tBOOH can be correlated with elevated levels of CcsR RNAs, as demonstrated by zone-of-inhibition assays. Filter disks soaked with either 200 mM paraquat or 700 mM tBOOH were placed on agar plates to suppress bacterial growth. *R. sphaeroides* wild-type strains carrying plasmid pRK415 or CcsR overexpression plasmids were compared. After 3 days of incubation, the diameters of the zones of inhibition were measured. Results represent the mean and error bars indicate the standard deviation for three independent biological replicates. Asterisks indicate a significant difference in the average zone of inhibition diameter.

dehydrogenase complex was decreased, which is in agreement with the microarray results. We observed different rates of synthesis of the hypothetical proteins RSP_2876 and RSP_2879, which are encoded by genes located in an operon together with *coxL*, and of PdhAa, which is encoded by a gene located in an operon with *pdhAb* and *pdhB*. From these data, we concluded that CcsR1–4 possibly have a function in the regulation of C_1 metabolism and the pyruvate dehydrogenase complex.

Our next step was to search for putative sites of CcsR1–4 interaction with mRNAs of the functionally related genes by using the web-based prediction tools IntaRNA for CcsR1–4 and RNApredator for CcsR1 to increase the reliability of the predictions (38, 39). First of all, these predictions indicated binding of CcsR1–4 to the same target mRNAs, which is why CcsR1 was consequently used as a representative for the analysis of the bioinformatic predictions (see Table S4 in the supplemental material). The results revealed that only parts of the interactions predicted by the two prediction tools overlapped the data derived from the microarray and proteome analyses. These overlaps finally represented a condensed set of putative target mRNA candidates and comprised RSP_2876, *coxL* (RSP_2877), *pdhB* (RSP_4050), and *pqqA* (RSP_6132), which were all shown to be downregulated on either the mRNA or the protein synthesis level (Table 1). In addition, *flhR* (RSP_2591) was of particular interest because of prediction results and its potential influence on C_1 metabolism through regulation of the *adhI-cycI* operon and through a putative role in the regulation of the *cycB-xoxJ* operon. Interestingly, the mRNAs/proteins encoded by the three genes *adhI*, *cycB*, and *xoxJ* were

TABLE 1 Combination of transcriptome and proteome analyses of CcsR1–4 overexpression and bioinformatic RNA interaction predictions reveals putative CcsR target genes[a]

Gene	Energy (kcal/mol)		Other gene(s) in operon, position in operon	Function	Log_2 fold change in *R. sphaeroides* 2.4.1(prk415) vs *R. sphaeroides* 2.4.1(pRCcsr1–4)	
	IntaRNA CcsR1	RNApredator CcsR1			Transcriptome	Proteome
Top 10 genes in prediction						
RSP_6040	−27.4	−22.7	1	Hypothetical protein	0.03	
RSP_2255	−22.7		2	Acyl coenzyme A synthase	−0.07	
			RSP_2254, 1	ABC efflux transporter, fused ATPase and inner membrane subunits	−0.16	
RSP_3500	−22.5		4	ABC sugar transporter, periplasmic binding protein	0.06	
			RSP_3503, 1	Sugar ABC transporter ATPase	−0.06	
			RSP_3502, 2	ABC sugar transporter, inner membrane subunit	0.12	
			RSP_3501, 3	ABC sugar transporter, inner membrane subunit	0.02	
			RSP_3499, 5	Short-chain dehydrogenase	0.29	
RSP_3949 (*ansB*)	−22.4		1	Asparaginase/glutaminase	0.15	
			RSP_3947, 2	GntR family transcriptional regulator	0.11	
RSP_1576 (*trxB*)	−22	−19.59	1	Thioredoxin reductase	−0.11	
RSP_2591 (*flhR*)	−21.8	−20.26	1	Two-component transcriptional regulator, LuxR family	−0.31	
			RSP_2592, 2	Hypothetical protein	−0.09	
			RSP_2593 (*flhS*), 3	Hybrid histidine kinase	−0.17	
RSP_1195 (*comF*)	−21.7		1	Competence protein F	0.29	
			RSP_1194 (*grxC*), 2	Glutaredoxin	−0.11	
RSP_2749	−21.5			Putative P4 family integrase	0.12	
RSP_2872 (*aglF*)	−21.4	−20.17	2	ABC α-glucoside transporter, inner membrane subunit AglF	0.07	
			RSP_2870, 4	ABC α-glucoside transporter, ATPase subunit AglK	0.04	
			RSP_2871, 3	ABC α-glucoside transporter, inner membrane subunit AglG	0.06	
			RSP_2873, 1	ABC α-glucoside transporter, perplasmic substrate-binding protein	0.01	
RSP_0573 (*phoB*)	−21.2	−19.86	5	Response regulator receiver protein	0.06	
			RSP_0572, 6	Putative exonuclease	0.01	
			RSP_0574, 4	Hypothetical protein	−0.17	
			RSP_0575, 3	Predicted signal transduction protein containing cyclic nucleotide-binding and CBS domains	0.04	
			RSP_0576, 2	Na^+/solute symporter	−0.34	
			RSP_0577, 1	Hypothetical protein	−0.42	
Genes with good correlation of bioinformatic predictions and gene expression data						
RSP_6132 (*pqqA*)	−19.7	−17.96	1	Putative coenzyme PQQ synthesis protein A	−1,19	
			RSP_0792, 3	PQQ biosynthesis protein PqqC	−0.27	
			RSP_0793, 2	PQQ biosynthesis protein PqqB	−0.25	
RSP_4050 (*pdhB*)	−18.2		3	Dihydrolipoamide acetyltransferase component (E2) of pyruvate dehydrogenase complex	−0.78	
			RSP_4047 (*pdhAa*), 1	Pyruvate dehydrogenase E1 component, α subunit	−0.61	−0.88
			RSP_4049 (*pdhAb*), 2	Dihydrolipoamide acetyltransferase	−0.87	
RSP_2876	−18.4		4	Putative carbon monoxide dehydrogenase medium chain	−0.39	−0.53

(Continued on following page)

TABLE 1 (Continued)

Gene	Energy (kcal/mol) IntaRNA CcsR1	Energy (kcal/mol) RNApredator CcsR1	Other gene(s) in operon, position in operon	Function	Log_2 fold change in *R. sphaeroides* 2.4.1(prk415) vs *R. sphaeroides* 2.4.1(pRCcsr1–4) Transcriptome	Proteome
RSP_2877 (*coxL*)	−16.2		3	Putative carbon monoxide dehydrogenase large chain	−0.72	−0.36
			RSP_2878 (*coxS*), 2	Putative carbon monoxide dehydrogenase small chain	−0.81	
			RSP_2879, 1	Hypothetical protein	−0.55	−0.92
Selected genes with changed expression			RSP_2575, 1	Glutathione-dependent formaldehyde-activating enzyme	−0.24	
			RSP_2576 (*adhI*), 2	Alcohol dehydrogenase class III	−0.43	−0.31
			RSP_2577 (*cycI*), 3	Isocytochrome c_2	−0.48	
			RSP_2578 (*xoxF*), 1	Putative pqq dehydrogenase protein	−0.96	
			RSP_2579 (*cycB*), 2	Cytochrome c_{553i}	−0.75	
			RSP_2580 (*xoxJ*), 3	Putative methanol oxidation protein	−0.77	
			RSP_2581, 4	Rhodanese	−0.38	

[a] Depicted are data from a transcriptome analysis and a gel-based proteome analysis comparing *R. sphaeroides* 2.4.1(pRCcsr1–4) to the control strain *R. sphaeroides* 2.4.1(pRK415) under aerobic conditions in the early exponential growth phase in comparison to bioinformatic predictions of CcsR target mRNAs. For the transcriptome analysis, two individual microarrays (biological replicates), each containing a pool of three independent experiments for each strain, were used. Genes were considered to be differentially expressed when the log_2 ratio was ≥0.7 or ≤−0.7. For the gel-based proteome analysis, three individual cultures of each strain were labeled with L-[^{35}S]methionine for 10 min to monitor changes in protein synthesis. Proteins with a significant change in their log_2 ratio were included (log_2 ≥0.3 and P≤ 0.05 or ≤−0.3 and P ≤ 0.05). The bioinformatic predictions for CcsR1 target mRNAs were performed by IntaRNA and RNApredator. For analysis of operons, ProOpDB was used (40).

among those downregulated and might therefore represent indirect targets of the CcsR sRNAs.

Confirmation of CcsR1–4-dependent regulation of predicted mRNA interaction partners *in vivo*. To investigate the binding of CcsR1–4 to putative target mRNAs, an *in vivo* RNA interaction reporter system for analysis in *R. sphaeroides* was used. The sRNAs CcsR1–4 were constitutively overexpressed under the control of a strong *R. sphaeroides* 2.4.1 16S rRNA promoter on the medium-copy-number plasmid pBBR1MCS2 (Fig. 3A). Putative targets of CcsR1–4 were translationally fused to *lacZ* on the low-copy-number plasmid pPHU235 and expressed from the same 16S rRNA promoter (Fig. 3B). β-Galactosidase activities from reporter plasmids were measured in the sRNA overexpression strain and compared to those of a control strain harboring the empty vector. A strain containing a nonspecific *bchN* (RSP_0285) reporter was used as a negative control (4). We analyzed the effects of CcsR1–4 on the expression of the mRNAs for the transcriptional regulator *flhR* (RSP_2591), the

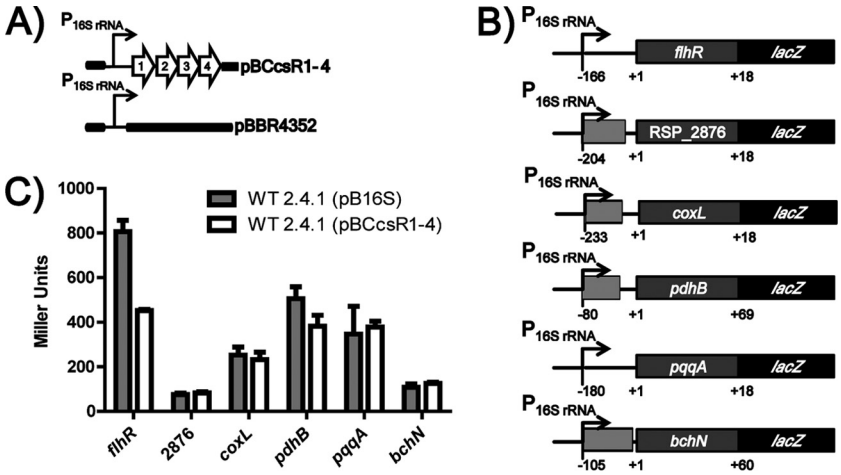

FIG 3 Effect of CcsR1–4 on the expression of putative target genes. (A) Graphical representation of CcsR1–4 overexpression plasmid pBCcsR1–4, which was used for the *in vivo* reporter system. Plasmid pBBR4352 served as a background control to measure basal β-galactosidase activity from reporter plasmids. Plasmids were transferred to wild-type *R. sphaeroides* 2.4.1 or an isogenic *hfq* deletion strain. (B) Construction of translational fusions of target mRNAs with *lacZ* on plasmid pPHU16S. The translational start of each target gene is the +1 position. Bases up- and downstream of the translational start site are displayed by negative and positive numbers, respectively. Additional genes in the upstream regions are indicated in light gray. (C) Relative β-galactosidase activities for translational *lacZ* fusions with *flhR* (RSP_2591), RSP_2876, *coxL* (RSP_2877), *pdhB* (RSP_4050), *pqqA* (RSP_6132), and *bchN* (RSP_0285). β-Galactosidase activities were measured in cell extracts from *R. sphaeroides* cultures in the exponential growth phase carrying either pBBR4352 or pBCcsR1–4. The *bchN′-′lacZ* fusion served as a nonspecific control. The error bars indicate the standard deviation from the mean of biological triplicates with two technical replicates each. WT, wild type.

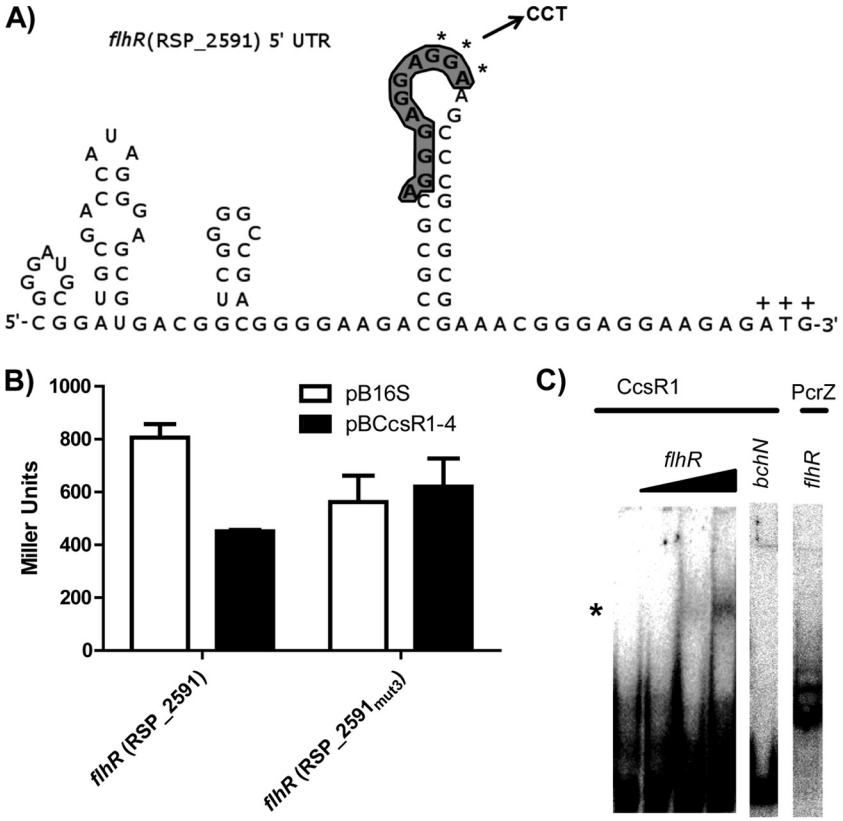

FIG 4 Effects of mutations in the predicted *flhR* binding site of CcsR1–4 and interaction of CcsR1 with the *flhR* mRNA *in vitro*. (A) The secondary structure of the *flhR* mRNA displays an exposed binding site for CcsR1 (bold and shaded) that is in relatively close proximity to the ATG codon (marked by plus signs). The bases selected for a triple mutation (GGA) are marked by asterisks, and the corresponding bases introduced for mutation (CCT) are displayed. Secondary structure was predicted by NUPACK (36). (B) A triple mutation within the predicted binding site of the *flhR* mRNA leads to loss of regulation by CcsR1–4 in the *in vivo* reporter system. The β-galactosidase activity was measured in cell extracts from *R. sphaeroides* cultures in the exponential growth phase carrying either pBBR4352 or pBCcsR1–4. (C) CcsR1 interacts with a 177-nt *flhR* mRNA fragment containing the predicted binging site already at low concentrations *in vitro*. A 250-fmol sample of CcsR1 was incubated with 25, 250, or 2,500 fmol of the *flhR* fragment and 2,500 fmol of the *bchN* control mRNA fragment, while 250 fmol of PcrZ (4) was incubated with 2,500 fmol of the *flhR* fragment. Changes in gel migration behavior were observable only for CcsR1 with the *flhR* fragment (marked by an asterisk), while no shift in the gel migration behavior of the controls was observable.

putative carbon monoxide dehydrogenase subunits *coxL* (RSP_2877) and RSP_2876, the pyruvate dehydrogenase subunit *pdhB* (RSP_4050), and *pqqA* (RSP_6132) encoding the PQQ coenzyme synthesis protein. For translational fusions with RSP_2876, *coxL* (RSP_2877) and *pqqA* (RSP_6132), no effect of CcsR1–4 overexpression was observable (Fig. 3C). For *pdhB* (RSP_4050), only a slight change in β-galactosidase activity of about 20% occurred. In contrast, the reporter plasmid for *flhR* (RSP_2591) gave rise to a strong and significant ($P < 0.05$) decrease in β-galactosidase activity of 50% in the CcsR1–4 overexpression strain (Fig. 3C). This indicates a direct inhibitory effect of the sRNAs on this mRNA.

Analysis of the interaction of CcsR1 with the *flhR* mRNA. To confirm the predicted site of interaction between sRNAs CcsR1–4 and *flhR* mRNA, a triple mutation was introduced into the *flhR'-'lacZ* fusion construct within the predicted CcsR1–4 binding site (Fig. 4A). After mutation of the *flhR* mRNA, the inhibitory effect of CcsR1–4 was no longer detectable (Fig. 4B). Testing of a compensatory mutation in the target was not possible, since such changes in the interaction site are predicted to severely change the RNA secondary structure. To further verify that CcsR1 interacts directly with the *flhR* mRNA, we performed gel shift assays. Radioactively labeled CcsR1 was transcribed *in vitro* and incubated with a 177-nt fragment of *flhR* mRNA. In the presence of the mRNA fragment, a change in the migration of CcsR1 was visible (Fig. 4C). When a fragment of the *bchN* mRNA, which has previously been shown to be targeted by the sRNA PcrZ in *R. sphaeroides* (4) but should not interact with CcsR1, was tested as a negative control, the CcsR1 migration remained unaffected. We also tested the effect of the *flhR* mRNA fragment on PcrZ and did not observe retardation of migration.

CcsR1–4-dependent repression of *flhR* increases the cellular GSH pool. FlhR is a transcriptional activator of GSH-dependent methanol/formaldehyde metabolism and may consequently influence the cellular GSH pool. Therefore, we compared the total GSH content of a CcsR1–4 overexpression strain with that of a control strain. Our results revealed that the CcsR1–4 overexpression strain has a higher GSH content per unit of OD_{660} (Fig. 5A). In a strain lacking FlhR, the GSH level was comparable to that of the wild type. Overexpression of CcsR1–4 in the mutant, however, failed to increase the GSH level (Fig. 5A). This supports the view that CcsR1–4 affect the GSH pool through the interaction with the *flhR* mRNA. In zone-of-inhibition assays, the *flhR* mutant showed resistance to oxidative stress similar to that of the wild type. Over-

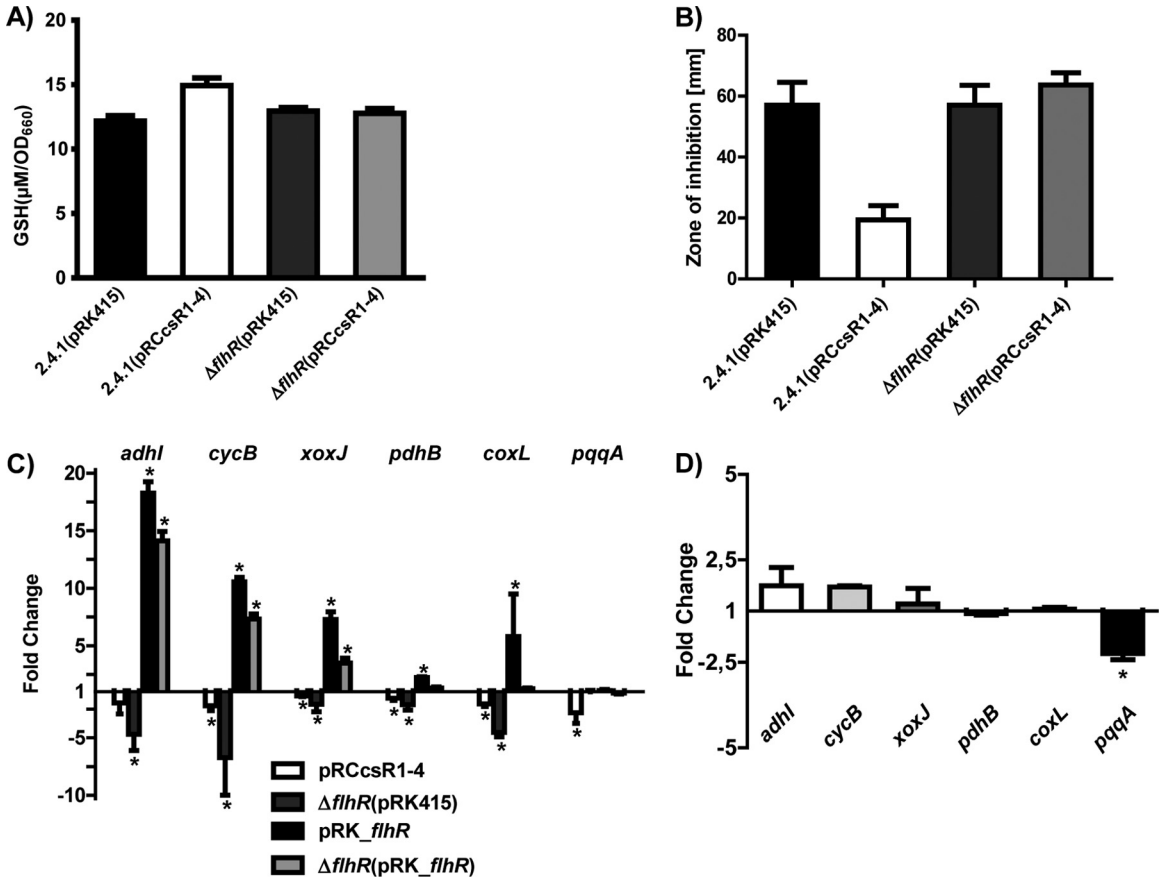

FIG 5 Comparison of CcsR1–4 functions in the wild-type and *flhR* deletion backgrounds. (A) Intracellular GSH was measured in wild-type 2.4.1 and an endogenous *flhR* deletion strain overexpressing CcsR1–4 (pRCcsR1–4), as well as in the respective control strains carrying the empty vector pRK415. The GSH concentration was determined in cell extracts from cultures in the exponential growth phase and normalized to the OD_{660}. The error bars indicate the standard deviation from the mean of biological triplicates with two technical replicates. (B) Enhanced resistance to oxidative stress promoted by CcsR1–4 overexpression is not observable in the endogenous *flhR* deletion strain, as demonstrated by zone-of-inhibition assays. Filter disks soaked with 700 mM tBOOH were placed on soft agar plates to suppress bacterial growth. Wild-type *R. sphaeroides* and an endogenous *flhR* mutant strain carrying plasmid pRK415 or pRCcsR1–4 were compared. After 3 days of incubation, the diameters of the zones of inhibition were measured. Results represent the mean and error bars indicate the standard deviation for three independent biological replicates. (C) Expression of selected genes from C_1 metabolism and *pdhB* determined by qRT-PCR in wild-type *R. sphaeroides* carrying the plasmid pRCcsR1–4 and in an endogenous *flhR* deletion strain. Moreover, wild-type *R. sphaeroides* carrying the plasmid pRK_*flhR* and the endogenous *flhR* deletion strain carrying the plasmid pRK_*flhR* were compared to wild-type *R. sphaeroides* carrying the empty plasmid pRK415. (D) CcsR1–4 overexpression in the *flhR* deletion strain does not lead to significantly changed expression of *pdhB* and most selected genes of C_1 metabolism, while only *pqqA* shows decreased expression, as determined by qRT-PCR. The error bars indicate the standard deviation of the mean of three biological replicates consisting of two technical replicates each. Asterisks indicate a statistically significant change in gene expression ($P \leq 0.05$).

expression of CcsR1–4 did not induce resistance to oxidative stress, as observed in the wild type (Fig. 5B). Finally selected genes from C_1 metabolism that displayed lower expression levels in the CcsR1–4 overexpression strain in the transcriptome analysis showed the same tendency of regulation when qRT-PCR was used (Fig. 5C). The genes from C_1 metabolism and *pdhB* also showed lower expression in the *flhR* deletion strain than in a control strain (Fig. 5C), indicating FlhR-dependent expression of *adhI*, *cycB*, *xoxJ*, *pdhB*, and *coxL*. Consequently, in the *flhR* deletion strain, overexpression of the CcsR RNAs from a plasmid did not have a significant impact on the expression of these selected genes from C_1 metabolism (Fig. 5D). Expression of *pqqA* and the effect of CcsR1–4 on *pqqA* mRNA levels were independent of FlhR.

DISCUSSION

Several sRNAs that are induced under (photo-)oxidative stress (20) were identified in the phototrophic alphaproteobacterium *R. sphaeroides* 2.4.1. Among these are the homologous sRNAs CcsR1–4, which are cotranscribed with the hypothetical protein RSP_6037. A tandem duplicate sRNA is involved in iron homeostasis in *Pseudomonas aeruginosa*, and sRNA tandem repeats from type III toxin-antitoxin systems in *Erwinia carotovora* are also known (45, 46). However, in the special case of CcsR1–4, the sRNAs are derived from the 3′ UTR of the upstream gene (RSP_6037). 3′ UTR-derived sRNAs were also demonstrated for other organisms like *E. coli* and *Salmonella enterica* serovar Typhimurium and might therefore be more common (20, 47, 48). We identified conditions that induce CcsR1–4 and RSs1543, which have not been described until now for $RpoH_I/RpoH_{II}$-dependent genes, indicating that the $RpoH_I/RpoH_{II}$ regulon, in general, is induced under these conditions. Enhanced resistance to oxidative stress of a strain that overexpresses CcsR1–4 demonstrates a role in this stress response. A screening for putative target mRNAs was

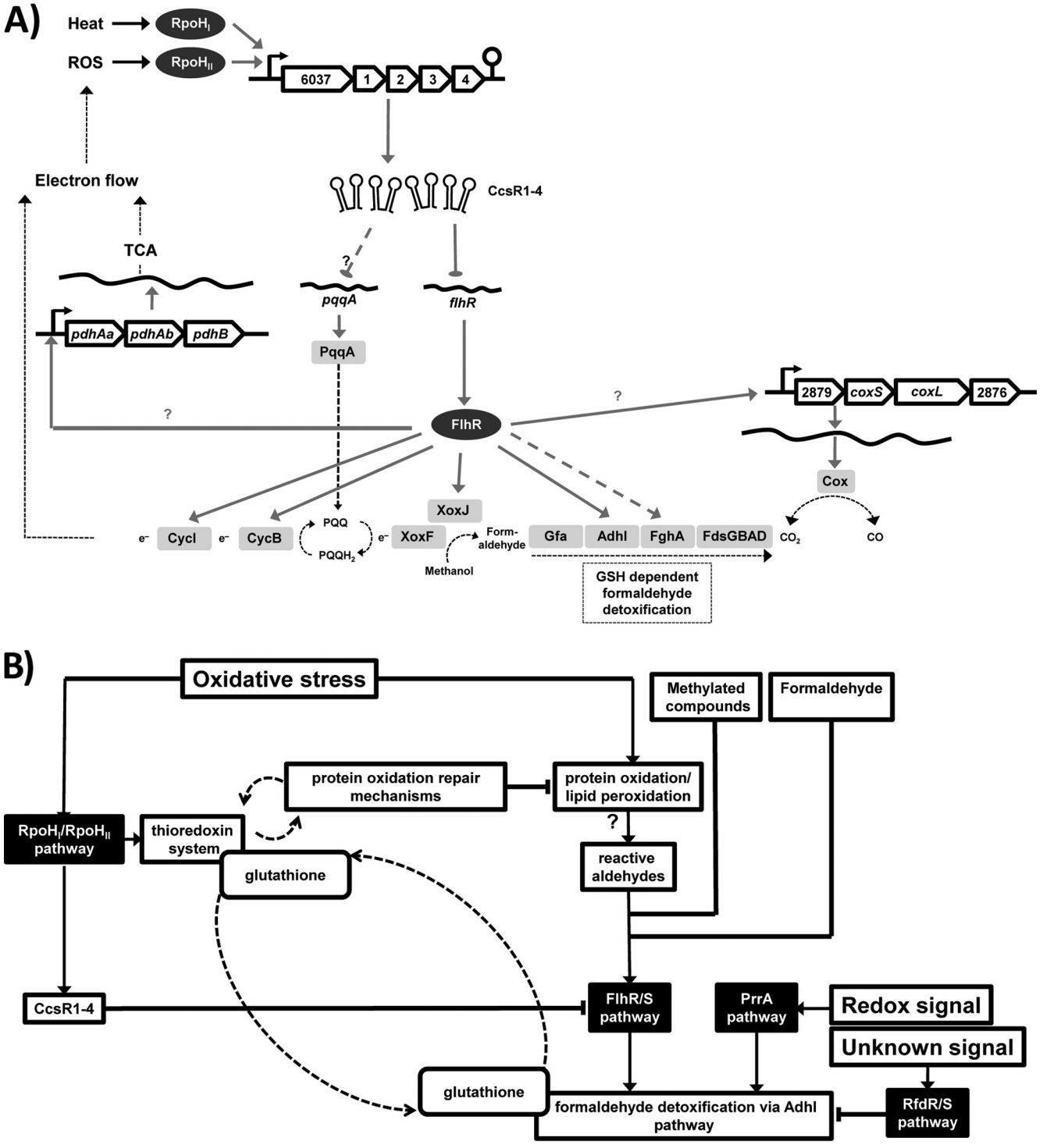

FIG 6 Metabolic network of CcsR-dependent targets and influence on cell regulatory networks. (A) After stress-dependent transcription, sRNAs CcsR1–4 repress *flhR* directly and thereby indirectly repress several genes with roles in C_1 metabolism and electron transport. Moreover, CcsR1–4 influence *pqqA* expression through an unknown mechanism. FlhR is a transcriptional activator that has been shown to regulate *adhI* and *cycI* in *R. sphaeroides* (53). *cycB* and *fghA* were demonstrated to be regulated by FlhR in *P. denitrificans* (55), while *xoxJ* is located in an operon together with *cycB* in *R. sphaeroides*. Moreover, *xoxJ* and *cycB* also show FlhR dependence in *R. sphaeroides* and a dependence of the pyruvate dehydrogenase complex gene *pdhB* on FlhR is indicated. XoxF and XoxJ are potential methanol oxidation proteins. TCA, tricarboxylic acid cycle. (B) Under oxidative stress, thioredoxins and GSH help to prevent oxidative protein and lipid damage by interacting directly with oxidized residues and CcsR1–4 lead to repression of *flhR*. Through this, the stimulation of the AdhI pathway is indirectly decreased. In addition, the AdhI pathway is known to be regulated by PrrA and RfdR (12, 53). If protein oxidation is not sufficiently prevented, protein carbonylation occurs and reactive aldehydes are produced. These reactive aldehydes probably lead to activation of *flhR* and more AdhI is produced, which then, with the help of GSH, takes on a putative protective role in the oxidative stress response (54). Through the influence of the CcsR RNAs, fine-tuning of GSH allocation in this network is achieved.

based on transcriptome and proteome analyses, as well as bioinformatic predictions. In the transcriptome analysis, the steady-state levels of a small number of the transcripts showed reduced levels upon CcsR1–4 overexpression, in agreement with a specific regulatory function of CcsR1–4 and implying an inhibitory effect, as observed for most *trans*-encoded sRNAs (14). Most genes with lowered mRNA levels are involved directly in C_1 metabolism, contribute to C_1 metabolism by cofactor synthesis, or encode subunits of the pyruvate dehydrogenase complex. Changes in the synthesis of proteins involved in the metabolic pathways mentioned were confirmed by the proteomic approach. Overlap of the different bioinformatic target predictions by IntaRNA and RNApredator was limited to interaction predictions where CcsR1–4 bind to the same target mRNAs. We conclude that the four copies of the CcsR RNAs possibly show functional redundancy by binding to the same target mRNA and thereby enhance the efficiency of regulation by increasing the ratio of sRNA molecules to mRNA molecules. This is supported by the observation that all four sRNAs are needed for maximum induction of resistance to oxidative stress in inhibition zone assays. A similar observation, that homologous sRNAs can have functional redundancy and bind to the same mRNA, was made before for, e.g., the sRNAs PrrF1 and PrrF2 from *P. aeruginosa*, for OmrA and OmrB in *E. coli*, and for the Qrr sRNAs in *Vibrio cholerae* (45, 49–52). The integration of our data suggests that CcsR1–4 indirectly affect C_1 metabolism by binding the mRNA of the transcriptional regulator FlhR. FlhR is a LuxR family transcriptional activator that activates the transcription of *adhI* and *cycI* upon exposure to formaldehyde and methylated compounds as part of a regulatory network that additionally involves the central response regulator PrrA and the transcriptional repressor RfdR (12, 53). AdhI and CycI play a central role in GSH-dependent formaldehyde detoxification, and a function of class III alcohol dehydrogenases like AdhI in oxidative stress is established (13, 54). Moreover, it is known that the FlhR homolog in *Paracoccus denitrificans* is involved in the regulation of the *cycB-xoxJ* operon and *fdhA* (55). The loss of regulation through a triple-base mutation in the predicted binding site within the *flhR* mRNA and the observed interaction between CcsR1 and the respective region of the *flhR* mRNA *in vitro* support the predictions of CcsR1–4 binding to this specific region. The observed binding site of this interaction is located in a partially unpaired region of a stem-loop structure, which is in close upstream proximity to but does not overlap the ribosomal binding site (RBS) of *flhR*. Several sRNAs were shown to bind their targets upstream of the RBS and to interfere with translation by various mechanisms These include, e.g., translation inhibition of an upstream open reading frame combined with translational coupling, as shown for the regulation of *fur* mRNA by RyhB (56), blocking of the ribosome stand-by site of *tisB* mRNA by IstR1 (57), and GcvB binding to translational enhancer elements in several mRNAs (58). In agreement with the observed regulation of the transcriptional regulator FlhR, the effect of CcsR1–4 on expression of genes from C_1 metabolism is apparently indirect. Interestingly, all of the subunits of the pyruvate dehydrogenase complex were expressed less in the CcsR1–4 overexpression strain and in the *flhR* deletion strain, while no interaction of the *pdhB* mRNA with CcsR1–4 was observable. This indicates a direct or indirect effect of FlhR on the pyruvate dehydrogenase complex that has not been described before but also renders a direct interaction with CcsR1–4 unlikely. In addition to FlhR-dependent effects of CcsR1–4, an FlhR-independent influence of CcsR1–4 on *pqqA* expression was observed. The PqqA peptide is a precursor of PQQ, which is an important redox cofactor in Gram-negative bacteria and is functionally related to C_1 metabolism (59–61).

The repressing effect of CcsR1–4 on genes from C_1 metabolism gives rise to the question of physiological relevance. The increased resistance to oxidative stress of a CcsR1–4 overexpression strain already revealed an important role in the respective cellular response. But how is C_1 metabolism connected to oxidative stress? On the one hand, the regulation of PqqA and FlhR through the CcsR RNAs can lead to decreased stimulation of the respiratory electron transport chain, which is known to be a source of ROS formation. In this respect, reduced ATP production comes as a trade-off for reduced ROS formation (Fig. 6A). On the other hand, an influence of CcsR1–4 on GSH-dependent mechanisms is indicated. Here especially, the function of the AdhI pathway in oxidative stress seems to be of central importance, as a role for the type III alcohol dehydrogenase AdhE from *E. coli* in the oxidative stress response was demonstrated (54). AdhI most likely functions in GSH-dependent detoxification of reactive aldehydes that are formed in oxidative protein carbonylation through ROS. In the course of the oxidative stress response, the allocation of GSH is partly controlled through a ratio of the CcsR RNAs to the *flhR* mRNA. While CcsR1–4 are generally formed upon stress, they will act as a fast riboregulator on the *flhR* mRNA and lead to repression of FlhR, leading to inhibition of the GSH-dependent AdhI pathway. This leads to allocation of GSH to protein repair in concert with the thioredoxin system. Continuing protein oxidation will lead to protein carbonylation and, related to this, to the formation of reactive aldehydes. The reactive aldehydes possibly induce *flhR* expression and thereby the expression of genes of the AdhI pathway. GSH will be allocated to the AdhI pathway as long as FlhR expression is stimulated and reactive aldehydes are glutathionylated. Consequently, a fraction of the intracellular GSH is bound to aldehydes and not available for the initial protein repair mechanism but prevents a toxic effect of accumulating aldehydes. Thus, depending on the nature of the oxidative protein damage that occurs, fine-tuning of *flhR* expression by CcsR1–4 leads to precisely regulated GSH allocation to different cellular mechanisms that handle the oxidative damage (Fig. 6B).

ACKNOWLEDGMENTS

We thank Yannick Hermanns and Kerstin Haberzettl for help with plasmid construction. Esther Jortzik is acknowledged for discussion of GSH measurements.

Funding was provided by the DFG Priority Program SPP1258 Sensory and Regulatory RNAs in Prokaryotes to G. Klug. F. Billenkamp was an associated member of the DFG IRTG 1384 Enzymes and Multienzyme Complexes Acting on Nucleic Acids.

REFERENCES

1. **Gregor J, Klug G.** 1999. Regulation of bacterial photosynthesis genes by oxygen and light. FEMS Microbiol Lett **179:**1–9. http://dx.doi.org/10.1111/j.1574-6968.1999.tb08700.x.
2. **Pemberton JM, Horne IM, McEwan AG.** 1998. Regulation of photosynthetic gene expression in purple bacteria. Microbiology **144:**267–278. http://dx.doi.org/10.1099/00221287-144-2-267.
3. **Klug G.** 1991. Endonucleolytic degradation of *puf* mRNA in *Rhodobacter capsulatus* is influenced by oxygen. Proc Natl Acad Sci U S A **88:**1765–1769. http://dx.doi.org/10.1073/pnas.88.5.1765.
4. **Mank NN, Berghoff BA, Hermanns YN, Klug G.** 2012. Regulation of

bacterial photosynthesis genes by the small noncoding RNA PcrZ. Proc Natl Acad Sci U S A **109:**16306–16311. http://dx.doi.org/10.1073/pnas.1207067109.
5. **Davies KJ.** 1995. Oxidative stress: the paradox of aerobic life. Biochem Soc Symp **61:**1–31.
6. **Arellano JB, Yousef YA, Melø TB, Mohamad SBB, Cogdell RJ, Naqvi KR.** 2007. Formation and geminate quenching of singlet oxygen in purple bacterial reaction center. J Photochem Photobiol B Biol **87:**105–112. http://dx.doi.org/10.1016/j.jphotobiol.2007.03.004.
7. **Uchoa AF, Knox PP, Turchielle R, Seifullina NK, Baptista MS.** 2008. Singlet oxygen generation in the reaction centers of *Rhodobacter sphaeroides*. Eur Biophys J **37:**843–850. http://dx.doi.org/10.1007/s00249-008-0287-y.
8. **Glaeser J, Nuss AM, Berghoff BA, Klug G.** 2011. Singlet oxygen stress in microorganisms. Adv Microb Physiol **58:**141–173. http://dx.doi.org/10.1016/B978-0-12-381043-4.00004-0.
9. **Barber RD, Donohue TJ.** 1998. Function of a glutathione-dependent formaldehyde dehydrogenase in *Rhodobacter sphaeroides* formaldehyde oxidation and assimilation. Biochemistry **37:**530–537. http://dx.doi.org/10.1021/bi971463t.
10. **Quayle JR, Pfennig N.** 1975. Utilization of methanol by rhodospirillaceae. Arch Microbiol **102:**193–198. http://dx.doi.org/10.1007/BF00428368.
11. **Sahm H, Cox RB, Quayle JR.** 1976. Metabolism of methanol by *Rhodopseudomonas acidophila*. J Gen Microbiol **94:**313–322. http://dx.doi.org/10.1099/00221287-94-2-313.
12. **Barber RD, Donohue TJ.** 1998. Pathways for transcriptional activation of a glutathione-dependent formaldehyde dehydrogenase gene. J Mol Biol **280:**775–784. http://dx.doi.org/10.1006/jmbi.1998.1900.
13. **Wilson SM, Gleisten MP, Donohue TJ.** 2008. Identification of proteins involved in formaldehyde metabolism by *Rhodobacter sphaeroides*. Microbiology **154:**296–305. http://dx.doi.org/10.1099/mic.0.2007/011346-0.
14. **Waters LS, Storz G.** 2009. Regulatory RNAs in bacteria. Cell **136:**615–628. http://dx.doi.org/10.1016/j.cell.2009.01.043.
15. **Aiba H.** 2007. Mechanism of RNA silencing by Hfq-binding small RNAs. Curr Opin Microbiol **10:**134–139. http://dx.doi.org/10.1016/j.mib.2007.03.010.
16. **Brennan RG, Link TM.** 2007. Hfq structure, function and ligand binding. Curr Opin Microbiol **10:**125–133. http://dx.doi.org/10.1016/j.mib.2007.03.015.
17. **Valentin-Hansen P, Eriksen M, Udesen C.** 2004. The bacterial Sm-like protein Hfq: a key player in RNA transactions. Mol Microbiol **51:**1525–1533. http://dx.doi.org/10.1111/j.1365-2958.2003.03935.x.
18. **Wagner EG.** 2013. Cycling of RNAs on Hfq. RNA Biol **10:**619–626. http://dx.doi.org/10.4161/rna.24044.
19. **Sharma CM, Hoffmann S, Darfeuille F, Reignier J, Findeisz S, Sittka A, Chabas S, Reiche K, Hackermuller J, Reinhardt R, Stadler PF, Vogel J.** 2010. The primary transcriptome of the major human pathogen *Helicobacter pylori*. Nature **464:**250–255. http://dx.doi.org/10.1038/nature08756.
20. **Berghoff BA, Glaeser J, Sharma CM, Vogel J, Klug G.** 2009. Photooxidative stress-induced and abundant small RNAs in *Rhodobacter sphaeroides*. Mol Microbiol **74:**1497–1512. http://dx.doi.org/10.1111/j.1365-2958.2009.06949.x.
21. **Nuss AM, Glaeser J, Berghoff BA, Klug G.** 2010. Overlapping alternative sigma factor regulons in the response to singlet oxygen in *Rhodobacter sphaeroides*. J Bacteriol **192:**2613–2623. http://dx.doi.org/10.1128/JB.01605-09.
22. **Vieira J, Messing J.** 1982. The pUC plasmids, an M13mp7-derived system for insertion mutagenesis and sequencing with synthetic universal primers. Gene **19:**259–268. http://dx.doi.org/10.1016/0378-1119(82)90015-4.
23. **Hübner P, Masepohl B, Klipp W, Bickle TA.** 1993. *nif* gene expression studies in *Rhodobacter capsulatus*: *ntrC*-independent repression by high ammonium concentrations. Mol Microbiol **10:**123–132. http://dx.doi.org/10.1111/j.1365-2958.1993.tb00909.x.
24. **Hübner P, Willison JC, Vignais PM, Bickle TA.** 1991. Expression of regulatory *nif* genes in *Rhodobacter capsulatus*. J Bacteriol **173:**2993–2999.
25. **Drews G.** 1983. Mikrobiologisches Praktikum. Springer-Verlag, Berlin, Germany.
26. **Glaeser J, Klug G.** 2005. Photo-oxidative stress in *Rhodobacter sphaeroides*: protective role of carotenoids and expression of selected genes. Microbiology **151:**1927–1938. http://dx.doi.org/10.1099/mic.0.27789-0.
27. **Janzon L, Löfdahl S, Arvidson S.** 1986. Evidence for a coordinate transcriptional control of alpha-toxin and protein a synthesis in *Staphylococcus aureus*. FEMS Microbiol Lett **33:**193–198. http://dx.doi.org/10.1111/j.1574-6968.1986.tb01270.x.
28. **Peuser V, Remes B, Klug G.** 2012. Role of the Irr protein in the regulation of iron metabolism in *Rhodobacter sphaeroides*. PLoS One **7:**e42231. http://dx.doi.org/10.1371/journal.pone.0042231.
29. **Church GM, Gilbert W.** 1984. Genomic sequencing. Proc Natl Acad Sci U S A **81:**1991–1995. http://dx.doi.org/10.1073/pnas.81.7.1991.
30. **Smyth GK, Speed T.** 2003. Normalization of cDNA microarray data. Methods **31:**265–273. http://dx.doi.org/10.1016/S1046-2023(03)00155-5.
31. **Glaeser J, Zobawa M, Lottspeich F, Klug G.** 2007. Protein synthesis patterns reveal a complex regulatory response to singlet oxygen in *Rhodobacter*. J Proteome Res **6:**2460–2471. http://dx.doi.org/10.1021/pr060624p.
32. **Berth M, Moser FM, Kolbe M, Bernhardt J.** 2007. The state of the art in the analysis of two-dimensional gel electrophoresis images. Appl Microbiol Biotechnol **76:**1223–1243. http://dx.doi.org/10.1007/s00253-007-1128-0.
33. **Ding Y, Chan CY, Lawrence CE.** 2004. Sfold web server for statistical folding and rational design of nucleic acids. Nucleic Acids Res **32:**W135–141. http://dx.doi.org/10.1093/nar/gkh449.
34. **Hofacker IL.** 2003. Vienna RNA secondary structure server. Nucleic Acids Res **31:**3429–3431. http://dx.doi.org/10.1093/nar/gkg599.
35. **Hofacker IL, Fontana W, Stadler PF, Bonhoeffer LS, Tacker M, Schuster P.** 1994. Fast folding and comparison of RNA secondary structures (the Vienna RNA package). Monatsh Chem **125:**167–188. http://dx.doi.org/10.1007/BF00818163.
36. **Zadeh JN, Steenberg CD, Bois JS, Wolfe BR, Pierce MB, Khan AR, Dirks RM, Pierce NA.** 2011. NUPACK: analysis and design of nucleic acid systems. J Comput Chem **32:**170–173. http://dx.doi.org/10.1002/jcc.21596.
37. **Beisel CL, Updegrove TB, Janson BJ, Storz G.** 2012. Multiple factors dictate target selection by Hfq-binding small RNAs. EMBO J **31:**1961–1974. http://dx.doi.org/10.1038/emboj.2012.52.
38. **Smith C, Heyne S, Richter AS, Will S, Backofen R.** 2010. Freiburg RNA Tools: a web server integrating INTARNA, EXPARNA and LOCARNA. Nucleic Acids Res **38:**W373–7. http://dx.doi.org/10.1093/nar/gkq316.
39. **Eggenhofer F, Tafer H, Stadler PF, Hofacker IL.** 2011. RNApredator: fast accessibility-based prediction of sRNA targets. Nucleic Acids Res **39:**W149. http://dx.doi.org/10.1093/nar/gkr467.
40. **Taboada B, Ciria R, Martinez-Guerrer CE, Merino E.** 2012. ProOpDB: Prokaryotic Operon DataBase. Nucleic Acids Res **40**(Database issue): D627–D631. http://dx.doi.org/10.1093/nar/gkr1020.
41. **Klug G, Jäger A, Heck C, Rauhut R.** 1997. Identification, sequence analysis, and expression of the *lepB* gene for a leader peptidase in *Rhodobacter capsulatus*. Mol Gen Genet **253:**666–673. http://dx.doi.org/10.1007/s004380050370.
42. **Miller JH.** 1972. Experiments in molecular genetics. Cold Spring Harbor Laboratory, Cold Spring Harbor, NY.
43. **Edgar R.** 2002. Gene Expression Omnibus: NCBI gene expression and hybridization array data repository. Nucleic Acids Res **30:**207–210. http://dx.doi.org/10.1093/nar/30.1.207.
44. **Berghoff BA, Glaeser J, Sharma CM, Zobawa M, Lottspeich F, Vogel J, Klug G.** 2011. Contribution of Hfq to photooxidative stress resistance and global regulation in *Rhodobacter sphaeroides*. Mol Microbiol **80:**1479–1495. http://dx.doi.org/10.1111/j.1365-2958.2011.07658.x.
45. **Wilderman PJ, Sowa NA, FitzGerald DJ, FitzGerald PC, Gottesman S, Ochsner UA, Vasil ML.** 2004. Identification of tandem duplicate regulatory small RNAs in *Pseudomonas aeruginosa* involved in iron homeostasis. Proc Natl Acad Sci U S A **101:**9792–9797. http://dx.doi.org/10.1073/pnas.0403423101.
46. **Fineran PC, Blower TR, Foulds IJ, Humphreys DP, Lilley KS, Salmond GPC.** 2009. The phage abortive infection system, ToxIN, functions as a protein-RNA toxin-antitoxin pair. Proc Natl Acad Sci U S A **106:**894–899. http://dx.doi.org/10.1073/pnas.0808832106.
47. **Kawano M, Reynolds AA, Miranda-Rios J, Storz G.** 2005. Detection of 5′- and 3′-UTR-derived small RNAs and cis-encoded antisense RNAs in *Escherichia coli*. Nucleic Acids Res **33:**1040–1050. http://dx.doi.org/10.1093/nar/gki256.
48. **Chao Y, Papenfort K, Reinhardt R, Sharma CM, Vogel J.** 2012. An atlas of Hfq-bound transcripts reveals 3′ UTRs as a genomic reservoir of regulatory small RNAs. EMBO J **31:**4005–4019. http://dx.doi.org/10.1038/emboj.2012.229.
49. **Guillier M, Gottesman S.** 2006. Remodelling of the *Escherichia coli* outer membrane by two small regulatory RNAs. Mol Microbiol **59:**231–247. http://dx.doi.org/10.1111/j.1365-2958.2005.04929.x.

50. **Guillier M, Gottesman S.** 2008. The 5′ end of two redundant sRNAs is involved in the regulation of multiple targets, including their own regulator. Nucleic Acids Res **36:**6781–6794. http://dx.doi.org/10.1093/nar/gkn742.
51. **Holmqvist E, Reimegård J, Sterk M, Grantcharova N, Römling U, Wagner EGH.** 2010. Two antisense RNAs target the transcriptional regulator CsgD to inhibit curli synthesis. EMBO J **29:**1840–1850. http://dx.doi.org/10.1038/emboj.2010.73.
52. **Lenz DH, Miller MB, Zhu J, Kulkarni RV, Bassler BL.** 2005. CsrA and three redundant small RNAs regulate quorum sensing in *Vibrio cholerae*. Mol Microbiol **58:**1186–1202. http://dx.doi.org/10.1111/j.1365-2958.2005.04902.x.
53. **Hickman JW, Witthuhn VC, Dominguez M, Donohue TJ.** 2004. Positive and negative transcriptional regulators of glutathione-dependent formaldehyde metabolism. J Bacteriol **186:**7914–7925. http://dx.doi.org/10.1128/JB.186.23.7914-7925.2004.
54. **Echave P, Tamarit J, Cabiscol E, Ros J.** 2003. Novel antioxidant role of alcohol dehydrogenase E from *Escherichia coli*. J Biol Chem **278:**30193–30198. http://dx.doi.org/10.1074/jbc.M304351200.
55. **Harms N, Reijnders WN, Koning S, van Spanning RJ.** 2001. Two-component system that regulates methanol and formaldehyde oxidation in *Paracoccus denitrificans*. J Bacteriol **183:**664–670. http://dx.doi.org/10.1128/JB.183.2.664-670.2001.
56. **Vecerek B, Moll I, Bläsi U.** 2007. Control of Fur synthesis by the non-coding RNA RyhB and iron-responsive decoding. EMBO J **26:**965–975. http://dx.doi.org/10.1038/sj.emboj.7601553.
57. **Darfeuille F, Unoson C, Vogel J, Wagner EG.** 2007. An antisense RNA inhibits translation by competing with standby ribosomes. Mol Cell **26:**381–392. http://dx.doi.org/10.1016/j.molcel.2007.04.003.
58. **Sharma CM, Darfeuille F, Plantinga TH, Vogel J.** 2007. A small RNA regulates multiple ABC transporter mRNAs by targeting C/A-rich elements inside and upstream of ribosome-binding sites. Genes Dev **21:**2804–2817. http://dx.doi.org/10.1101/gad.447207.
59. **Anthony C.** 2001. Pyrroloquinoline quinone (PQQ) and quinoprotein enzymes. Antioxid Redox Signal **3:**757–774. http://dx.doi.org/10.1089/15230860152664966.
60. **Goosen N, Huinen RG, van de Putte P.** 1992. A 24-amino-acid polypeptide is essential for the biosynthesis of the coenzyme pyrroloquinoline-quinone. J Bacteriol **174:**1426–1427.
61. **Shen Y, Bonnot F, Imsand EM, RoseFigura JM, Sjölander K, Klinman JP.** 2012. Distribution and properties of the genes encoding the biosynthesis of the bacterial cofactor, pyrroloquinoline quinone. Biochemistry **51:**2265–2275. http://dx.doi.org/10.1021/bi201763d.